JOURNAL OF KUFA–PHYSICS
journal.uokufa.edu.iq/index.php/jkp/index | ISSN: 2077–5830

Effect of doping Zn into Sb_2Te_3 on the structural and optical properties by thermal Evaporation

***Jabbar A. Hamza[1], Firas A. Najim[1]**

University of Al-Qadisiyah, Al-Diwaniyah, IRAQ College of Education, [1]Department of Physics,

*Corresponding Author Email: **phy.edu.post24.14@qu.edu.iq** **

firas.najim@qu.edu.iq

ARTICLE INF.

Article history:
Received: 11 JAN., 2026
Revised: 01 MAR., 2026
Accepted: 03 MAR., 2026
Available Online: 28 JUN., 2026

Keywords:

Sb_2Te_3 thin films;
Optical properties;
Structural characteristics,
Thermal Evaporation

ABSTRACT

In this work, a thermal vacuum evaporation-based synthesis of pure (Sb2Te3) and zinc-doped antimony telluride (Sb2Te3: Zn) thin films is investigated. Structural properties of films were examined at 3%, 5% and 7% zinc content and thickness of (100, 200 and 300 nm) and few samples were annealed at 100 °C during the processes, and the formation of a polycrystalline hexagonal structure with enhanced crystallinity following annealing was analyzed by X-ray diffraction. Zinc doping led to lattice contraction and a small shift in diffraction peaks. After annealing, SEM surface analysis showed homogeneous quasi-spherical grains with an increase in size and uniformity. The AFM exhibited decreased roughness after annealing. Though initially increased and subsequently lowered by zinc, optical measurements reflected a good visible absorption with energy gap growth after annealing, With doping and annealing, electrical properties showed an increased conduction and decreased activation energy, confirming p-type behavior. With 5% zinc doping and moderate annealing the structural, optical, and electrical characteristics were optimized, allowing for photovoltaic and thermoelectric applications.

DOI: https://doi.org/10.31257/2018/JKP/2026/v18.i1.22804

دراسة تأثير تشويب عنصر الزنك في تيلورايد الانتيمون على الخصائص التركيبية والبصرية بطريقة التبخير الحراري

جبار عبد نور حمزة, فراس عائد نجم*

قسم الفيزياء، كلية التربية، جامعة القادسية، الديوانية، العراق

الـــخُـــلاصـــة

في هذه الدراسة، تمّ بحث عملية تصنيع أغشية رقيقة من تيلوريد الأنتيمون النقي (Sb2Te3) والمطعم بالزنك (Sb2Te3:Zn) باستخدام التبخير الحراري الفراغي. دُرست الخصائص البنيوية للأغشية عند نسب زنك 3% و5% و7% وبسمك (100, 200,300nm). خضعت بعض العينات

الكلمات المفتاحية:

أغشية الانتيمون تيلورايد,
الخصائص البصرية,

للمعالجة الحرارية عند 100°C لمدة ساعة واحدة أثناء عملية التصنيع، وتمّ تحليل النتائج وجود بنية سداسية متعددة البلورات ذات بلورية محسّنة بعد المعالجة الحرارية باستخدام حيود الأشعة السينية. أدّى تطعيم الزنك إلى انكماش الشبكة البلورية وانزياح طفيف في قمم الحيود. بعد المعالجة الحرارية، أظهر تحليل سطح الأغشية باستخدام المجهر الإلكتروني الماسح (SEM) حبيبات شبه كروية متجانسة ذات حجم وتجانس أكبر. كما أظهر فحص المجهر الذري الماسح (AFM) انخفاضًا في خشونة السطح بعد المعالجة الحرارية. على الرغم من أن امتصاص الضوء المرئي ازداد في البداية ثم انخفض لاحقًا بفعل الزنك، إلا أن القياسات البصرية أظهرت امتصاصًا جيدًا للضوء المرئي مع زيادة في فجوة الطاقة بعد التلدين. ومع التطعيم والتلدين، أظهرت الخصائص الكهربائية زيادة في التوصيل وانخفاضًا في طاقة التنشيط، مما يؤكد سلوك النوع .p ومع تطعيم الزنك بنسبة 5% والتلدين المعتدل، تم تحسين الخصائص الهيكلية والبصرية والكهربائية، مما يسمح بتطبيقات الخلايا الكهروضوئية والحرارية.

الخصائص التركيبية,
التبخير الحراري

1. INTRODUCTION

In the early twentieth century there was interest in thin films preparation, and thin films are those materials that having very low thickness and do not exceed one micrometer [1]. They show peculiar physical properties over their bulk counterparts [2]. By these films, we have been able to study electronic transitions and crystal structures of semiconductors greatly, which have led to broad investigation on electronic and optical properties by semiconductors being extensively studied and become [3] a focal point for scientific research and a foundation for modern technology. In this context, second generation topological insulators (TIs) (e.g., Sb2Te3, Bi2Te3, and Bi2Se3) have been increasingly used for electronic, optical, and photonic applications of the broad energy spectrum, such as ultraviolet, visible, and infrared spectra in recent years [4-5]. These materials possess a few interesting characteristics as compared to those in conventional materials, namely narrow band gap and surface states [6]. Semiconductors with small band gap are promising candidates for thermoelectric conversion. Moreover, the Sb2Te3 compound has attracted significant interest in recent years as a potentially interesting material toward photovoltaic devices due to direct band gap and high optical absorption [7-8]. Thin films are unique by having physical and chemical properties of the material distinct from its bulk form attributed to their composition, thickness and properties can be altered using various preparation methods [9], ranging from thermal evaporation, sputtering [10-11], pulse laser deposition (PLD) [12], electrochemical deposition [13], metal organic chemical vapor deposition (MOCVD) [14], and molecular beam epitaxy (MBE) [15]. The thermal vacuum evaporation method is widely regarded as one of the most accurate methods for thin film preparation. The thin films prepared using the thermal vacuum evaporation method consist of several key steps, beginning with the transubstantiation of the material to be deposited in a vapor state due to an electric current flowing through it [16]. Then, The molecules that have shifted to a gaseous state transfer from the boat onto the glass substrate that has been constructed to be deposited on it, which makes a thin

layer on the material. Evaporation takes place gradually within the film, leading to an increasing accumulation of evaporated material on the surface. [17]. The thermal vacuum evaporation was used for the preparation of pure (Sb2Te3) and zinc-doped (Sb2Te3: Zn) films in this work. Such technique is said to be one of the most efficient and frequently used method for producing film with a high purity and clear structural homogeneity and does not emit ionizing radiation in the procedure.

2. Experimental Part

2.1 Preparation of Sb_2Te^3 thin films.

Both pure and doping with Zn Thermal evaporation was performed to produce (Sb2Te3) thin films using a pure (Sb2Te3) compound with 99.99% purity level in a high vacuum environment. All these films which were laid on glass substrates were thoroughly washed with distilled water and alcohol, treated in an ultrasonic apparatus for 15 min, dried, and prepared for evaporation. With a rotary pump and diffusion pump, a vacuum of 10-5 m bar was created, and the pressure was measured using both the Pirani and Penning scales. Films at thickness of 100, 200, and 300 nm were deposited.. The double evaporation (Co-Evaporation) method was used to create (Sb_2Te_3) films doped with zinc (Zn). This process involved filling molybdenum pots inside the same vacuum chamber with zinc material and an amount of Sb_2Te_3 that reached a thickness of 100 nm. Zinc was added to the Sb_2Te_3mass at weight percentages of 3%, 5%, and 7%; the weight technique was used to calculate the thickness. After the required pressure of 3.5 × 105 m bar was reached, an electric current was gradually applied to glass substrates to initiate deposition. This allowed the Sb2Te3 and Zn to evaporate at different electrode temperatures. Both the clean and doped films were annealed at 100°C for an hour.

2.2 Characterization and measurement

The form and morphology of the thin film samples were investigated by X-ray diffraction (XRD, Rigaku D/MAX 2200 PC) with Cu Kα radiation (λ = 0.154 nm). Additionally, elements were identified using field emission SEM and EDX, and roughness was measured using atomic force microscopy (AFM). The film thickness was determined using both a weight-based method and a most precise optical method based on interference in thin films. In the weight-based method, the film thickness (t) was calculated using the following relation:

$$t = \frac{m}{A_\rho} \quad \ldots\ldots\ldots\ldots\ldots\ldots (1)$$

The thickness of the film was determined using the weight method, which is not particularly accurate; an optical approach that depends on ray interference in thin films, such as a laser, can be utilized.

In the optical interference method, the thickness (t) satisfies the condition:

$$2nt = m\lambda \ldots\ldots\ldots\ldots\ldots (2)$$

For the optical features, a UV-1800 device was also utilized.

3. Results and discussion

3.1 The X-ray diffraction analysis

The XRD patterns of pure (Sb_2Te_3) and doped with Zn (Sb_2Te_3: Zn) thin films are displayed in Figure 1 and listed in Table 1. These films were annealed at 100°C for an hour. The diffraction peaks were identified using the JCPD data. The samples have a regular crystalline structure that resembles antimony telluride's distinctive hexagonal shape. According to the standard card for the material (JCPDS No. 15-0874), the pure (Sb_2Te_3) film had diffraction angles of (28.394°), (28.103), and (28.283°), which correspond to the crystal plane (015). This match suggests that the favored direction for the growth of the prepared films is the (015) crystallographic direction. To improve these films' thermoelectric qualities, post-annealing was done. The XRD patterns of films composed of (Sb_2Te_3:3%Zn), (Sb_2Te_3:5%Zn), and (Sb_2Te_3:7%Zn) were shown and analyzed. As the doping rises, we found a small shift in the peak positions toward higher angles. When doped with (7%), the diffraction angle steadily increased to (28.535°) from (28.394°) for the pure sample. Due to the entry of zinc atoms with a smaller atomic radius into the sites of antimony or tellurium atoms within the crystal lattice, which causes a slight contraction in the dimensions of the crystal cell, this slight shift shows a contraction in the interplanar spacing (d-spacing) [18].

3.2 Structural parameters

3.2.1 Average grain size (D)

For all undoped and doped (Sb_2Te_3) samples, the (015) plane with the highest intensity was used to calculate the mean grain size. The average crystallite sizes of produced thin films were estimated using the Debye-Scherrer equation [19].

$$D = \frac{k\lambda}{\beta \cos\theta} \quad \ldots\ldots\ldots\ldots\ldots\ldots(3)$$

Where :

K: represents the shape factor and its value is (0.94).

λ: X-ray wavelength (nm).

θ: diffraction angle in Braque's law.

β: is measured in radian (FWHM) (Full Width at Half Maximum).

Results in Table 2, illustrates how the average crystallite size increased when the doping ratio rose to (7%), reaching (16.50 nm) before annealing and (29.01 nm) after annealing. Prior to annealing, it was found that the average grain size gradually increased as thickness increased. Because thicker layers offer a favorable environment for the regular accumulation of atoms and the production of larger, most stable grains, this behavior suggests that the increase in the thickness improve the enhancement of crystal development. However, compared to non-annealed films, it was observed that the grain size value of films that underwent thermal annealing reduces, particularly at lower thicknesses. This can be explained by the possibility of partial disintegration of fine grains or their redistribution within the crystalline structure results from annealing at relatively low temperatures, which may not be adequate to enable complete

recrystallization and, as a result, lower the average grain size [20].

3.2.2 Lattice constant (a,c)

To calculate the width and height (a,c) of pure antimony telluride films and films doped with different zinc concentrations before and after annealing, Equation (2) was used [19]:

$$\frac{1}{d_{hkL}^2} = \frac{4}{3}\left(\frac{h^2+hk+k^2}{a^2}\right) + \frac{L^2}{C^2} \quad \ldots.(4)$$

Where:

d: crystal distance between planes, (h,k,l): Miller coefficients, a,b,c: represent lattice constants.

According to Table 2, it was discovered that the doped films had higher lattice constants than the standard test card values. Additionally, clean and doped films displayed similar characteristics both before and after annealing. According to previous research, small departures from the starting values indicates good crystallization, while greater differences indicates poor crystallization [21]. Additionally, it was observed that the lattice constants increased as the doping percentage increased. However, the values of the lattice constants varied slightly, tending to increase in some samples and decrease in others based on the annealing conditions and the amount of added zinc. Because zinc atoms have a smaller radius than antimony or tellurium atoms, they enter the lattice sites, causing a minor contraction in the crystal cell, as indicated by the tiny drop in lattice constants [22]. This causes the atoms to converge and the crystalline density to rise, which is in line with the XRD spectra's modest change in diffraction angles toward higher values.

3.2.3 Dislocation density (δ)

Using Equation (3), which is inversely proportional to the grain size ratio,the dislocation density in pure (Sb_2Te_3) and zinc-doped (Sb_2Te_3:Zn) thin films were obtained[19]:

$$\delta = \frac{1}{D^2_{av}} \quad \ldots\ldots(5)$$

D: represents the average particle size

As indicated in Table 2, the dislocation density decreases step by step with increasing thickness. This decrease is a result of the increased uniformity of the crystal structure with increasing thickness, thus the internal flaws and distortions decrease as the atoms are mostly free to move about in the crystal lattice. Nonetheless, a significant increase in dislocation density was observed after thermal annealing at 100 °C, most notably in the sample with the lowest thickness of 100 nm, which reached (8.46). This means that the dislocations are only partially displaced and not completely eliminated; thus annealing at relatively mild temperatures only has partial redistribution of dislocations [23]. For the zinc-doped (Zn) films a similar trend of relative general narrowing of dislocation density was observed with added thickness. Density values on a lower doping of (3%) were comparably larger at a thickness of 100 nm, achieving (8.45). This indicates that the introduction of zinc impurities initially disrupted the shape of the crystal lattice. However, the density reduced gradually to (3.67) at 300 nm thickness when the

doping percentage was increased up to (7%). This suggests that the higher doping percentage helped stabilize the structure by filling vacant sites or causing a more balanced atomic rearrangement. Nevertheless, the dislocation density dramatically dropped after the doped samples were annealed, reaching extremely low values of (1.19) with (7%) doping and a thickness of 300 nm. By encouraging grain growth and raising the degree of internal crystallization, both annealing and zinc doping have a twofold beneficial effect on enhancing the crystalline structure and minimizing distortions [24]. There was a correlation between variations in dislocation density and changes in lattice constants.

3.2.4 Number of crystals per unit area (N^o)

The number of crystals per unit area (N^o) was calculated using Equation (4) [19]:

$$N^o = \frac{t}{D^3_{av}} \quad \ldots\ldots \qquad (6)$$

D: represents the average particle size.

It is evident from examining the values of the number of crystals per unit area ($N^o \times 10^{12}\ m^{-2}$)

displayed in Table 2, that this number is strongly correlated with the grain size (D). Because there are fewer grain borders per unit area when the

grain size increases, there are fewer crystals. Higher values of N^o are seen in the unalloyed samples and prior to annealing, suggesting a highly precise and fractured structure in the crystalline formation because of the tiny grain size and the inadequate crystalline development following deposition. Most samples showed a considerable drop in N^o values following the annealing procedure, which suggests an improvement in crystalline order and an increase in the merging of tiny grains into bigger ones, which lowers the number of visible crystals per unit area. Regarding the doped samples, the change in N^o is dependent on the doping ratio; in certain samples, the formation of new growth centers causes a slight increase in the number of crystals at moderate doping ratios, while the disruption of the crystal lattice causes the values to start declining again at higher doping ratios beyond the optimal limit [25].

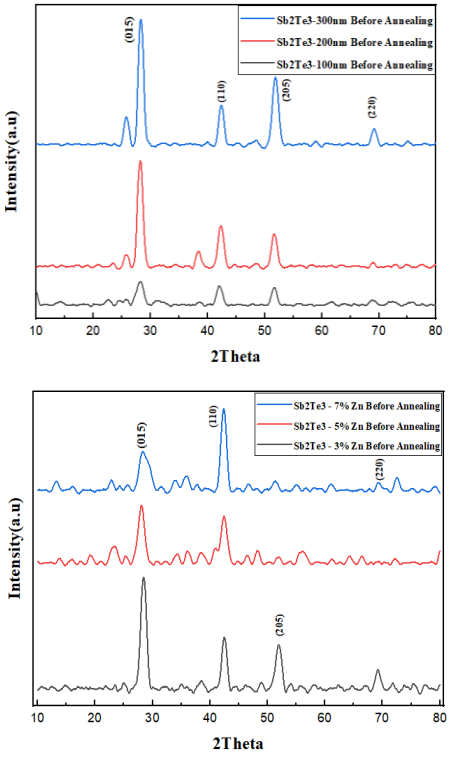

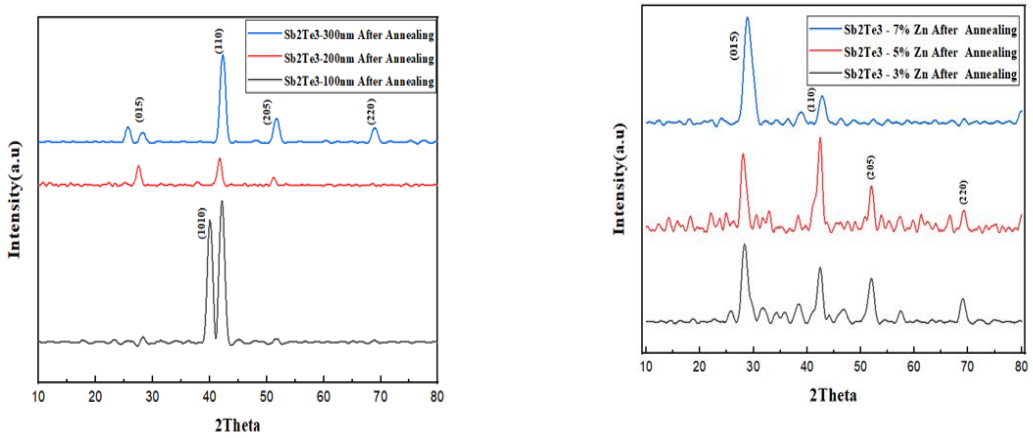

Figure 1. The XRD patterns for both pure Sb_2Te_3 and Sb_2Te_3 doped with Zn before and after annealing

Table 1. Results from X-ray diffraction for (Sb_2Te_3: Zn) films before and after annealing.

Sample	Annealing Temperature	2θ(degree)	d_{hkl} (Å)	FWHM (deg)	(hkl)
Pure Sb_2Te_3 (100 nm)	-	28.394	3.14337	0.590	(015)
Sb_2Te_3-3%Zn	-	28.519	3.12985	0.787	(015)
Sb_2Te_3-5%Zn	-	28.137	3.17144	0.590	(015)
Sb_2Te_3-7%Zn	-	28.535	3.11883	0.519	(015)
Sb_2Te_3-3%Zn	100 ℃	28.357	3.14736	0.295	(015)
Sb_2Te_3-5%Zn	100 ℃	28.078	3.19347	0.787	(015)
Sb_2Te_3-7%Zn	100 ℃	28.650	3.11325	0.480	(015)

Table 2. Results of the structural treatments of pure (Sb_2Te_3) films of different thicknesses and (Sb_2Te_3: Zn) before and after annealing and in the preferred growth direction (015).

Material	Thickness (nm)	Average Crystalline Size (Dav nm)	a=b XRD(A°)	c XRD(A°)	a=bStander (A°)	c Stander (A°)	$\delta \times 10^{10}$ (m^{-2})	$N_{0\times}10^{1}$ (m^{-2})
Sb_2Te_3	100	14.51	4.246	30.276	4.264	30.458	4.75	6.04
Sb_2Te_3	200	27.41	4.282	30.610	4.264	30.458	1.33	1.69

Sb_2Te_3	300	29.01	4.266	30.904	4.264	30.458	1.19	1.52
Sb_2Te_3	100/100°C	10.87	4.271	30.418	4.264	30.458	8.46	1.08
Sb_2Te_3	200/100°C	17.38	4.357	30.523	4.264	30.458	3.31	4.23
Sb_2Te_3	300/100°C	21.77	4.277	30.564	4.264	30.458	2.11	2.68
Sb_2Te_3: 3% Zn	100	10.88	4.228	30.146	4.264	30.458	8.45	1.08
Sb_2Te_3: 5% Zn	200	14.50	4.284	30.546	4.264	30.458	4.76	6.05
Sb_2Te_3: 7% Zn	300	16.50	4.213	30.037	4.264	30.458	3.67	4.67
Sb_2Te_3: 3% Zn	100/100°C	25.92	4.252	30.314	4.264	30.458	1.49	1.90
Sb_2Te_3: 5% Zn	200/100°C	28.64	4.314	30.758	4.264	30.458	1.22	1.55
Sb_2Te_3: 7% Zn	300/100°C	29.01	4.205	29.986	4.264	30.458	1.19	1.52

1.1 The SEM and EDX results

SEM images of (Sb_2Te_3) films with different thicknesses (100, 200, and 300 nm) before and after annealing are shown in Figure 2. Due to insufficient atomic mobility during deposition, surfaces are heterogeneous before annealing, with small, irregular grains and signs of roughness, gaps, and pores. After annealing, the surface morphology becomes much better because bigger, highly uniform grains form that lower porosity and eliminate of small gaps. This shows that the annealing process caused atoms to rearrange and grains to merge[26]. Figure 3 displays SEM images of (Sb_2Te_3: Zn) samples comprises fine granular clusters lacking before and afterannealing. Initially, the surface homogeneity, with some larger grains present. Zinc appears to influence crystal growth by promoting small nuclei formation, resulting in numerous fine grains of lesser size versus the pure sample. Post-annealing, grain uniformity and size increase, grain boundaries diminish, and fine gaps vanish, indicating enhanced atomic arrangement and grain coalescence [21]. The success of the doping process is confirmed by the energy-dispersive X-ray spectroscopy (EDX) examination of the (Sb_2Te_3: Zn) sample shown in Figure 3, which displays peaks for the zinc (Zn) alongside the Sb and Te peak

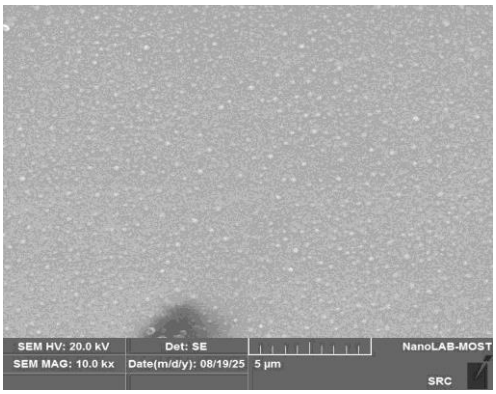

Sb_2Te_3 (100 nm) Before Annealing

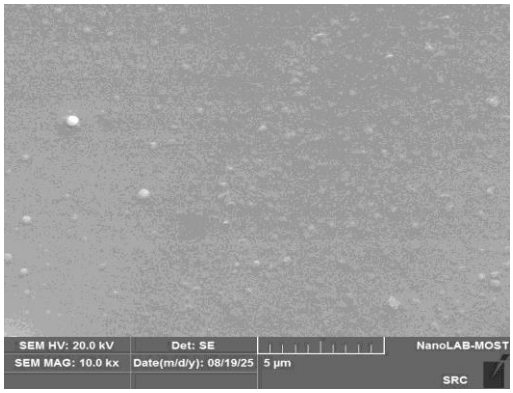

Sb_2Te_3 (200 nm) Before Annealing

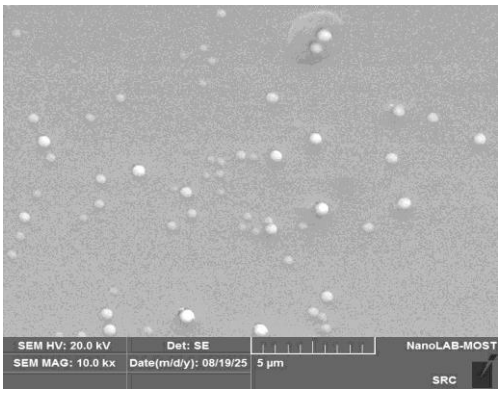

Sb_2Te_3 (300 nm) Before Annealing

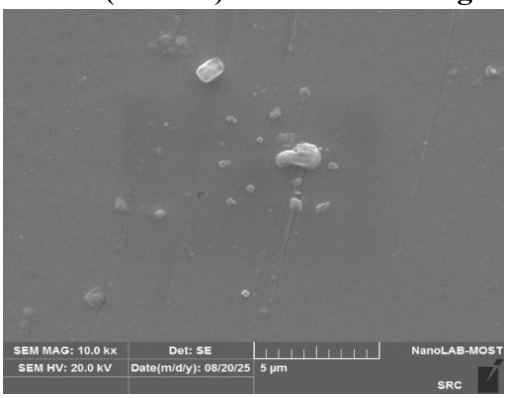

Sb_2Te_3 (100 nm) After Annealing

Figure 2. SEM images of pure Sb2Te3 films with thicknesses (100, 200 ,300 nm) before and after annealing.

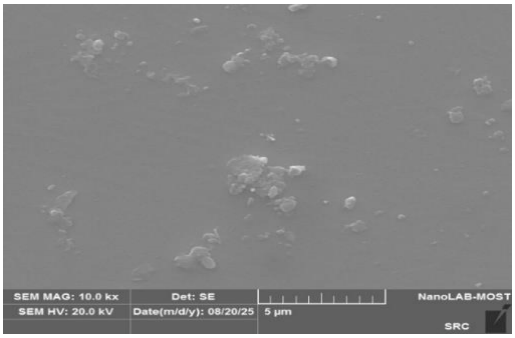

Sb_2Te_3 (200 nm) After Annealing

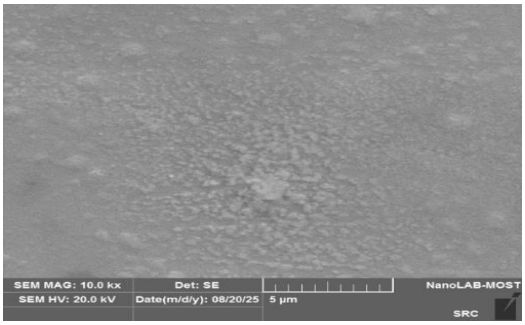

(Sb_2Te_3:3% Zn) Before Annealing

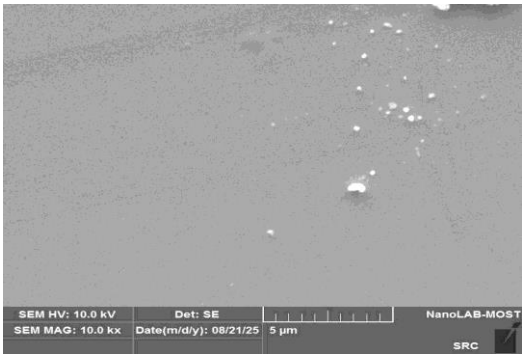

(Sb_2Te_3:5% Zn) Before Annealing

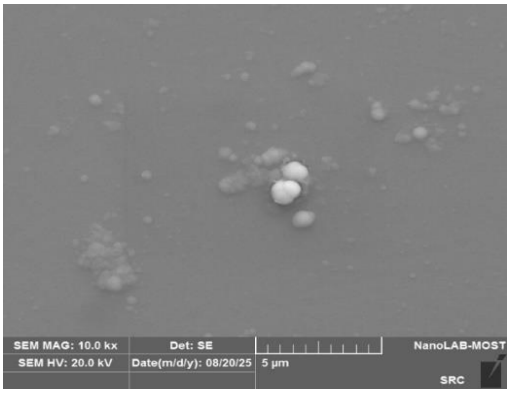

Sb_2Te_3 (300 nm) After Annealing

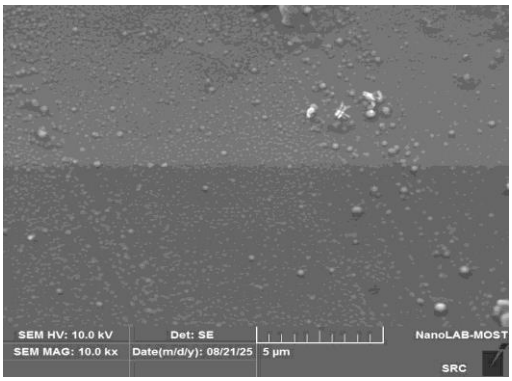

(Sb_2Te_3:7% Zn) Before Annealing

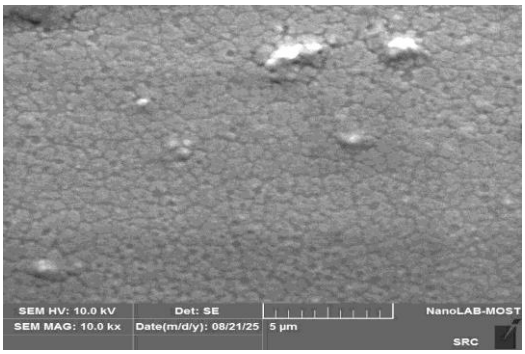

(Sb2Te3:3% Zn) After Annealing

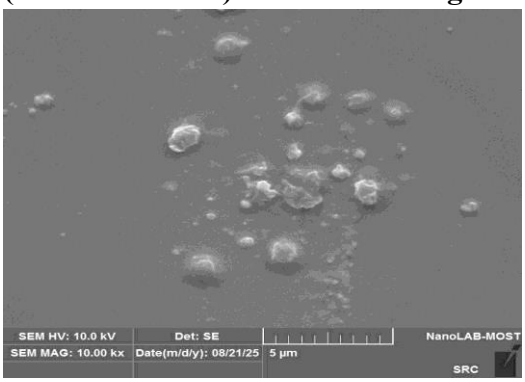

(Sb_2Te_3:5% Zn) After Annealing

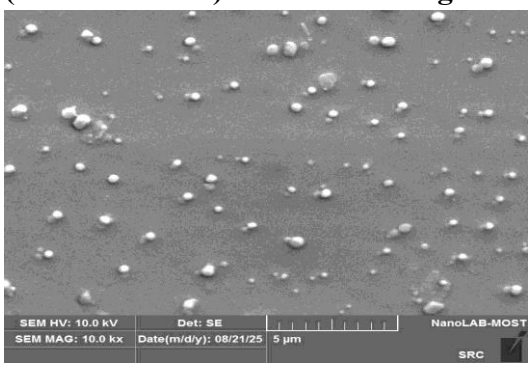

(Sb_2Te_3:7% Zn) After Annealing

Figure 3. SEM images of (Sb2Te3: Zn) films at concentrations of (3% ,5% .7%) before and after annealing and were also analyzed using EDX for elemental composition**.**

1.1 AFM results

Figure 4, shows the (AFM) images of (Sb_2Te_3) films before and after annealing for three thicknesses (100, 200, 300) nanometers. It was noted that as film thickness increases prior to annealing, the roughness average (Sa) and root mean square roughness (R.M.S) values rise and fall. The average roughness is (2.695 nm) for a layer thickness of 100 nm and (5.898 nm) for a thickness of 200 nm. Because of the decrease in crystalline boundaries and the increase in particle size, an increase in the roughness rate. The roughness rate is (2.176 nm) for a thickness of 300 nm, which shows a drop in the roughness rate as a result of a rise in crystalline boundaries and a decrease in grain size. Table 3 provides roughness values for the samples. However, with annealing, the thicknesses of 100 nm, 200 nm, and 300 nm have roughness rates of 2.073 nm, 2.054 nm, and 2.464 nm, respectively. Because surface atoms are stabilized and membrane homogeneity is improved, the annealing process improves the rearranging of atoms within the grains and decreases defects and internal stress, resulting in a decrease in roughness [27]. The (AFM) results of (Sb_2Te_3: Zn) films before and after annealing are displayed in Figure 5. Following annealing, the roughness rate falls in comparison to the pure films and also begins to decrease as the zinc doping ratio increases. The roughness rates for

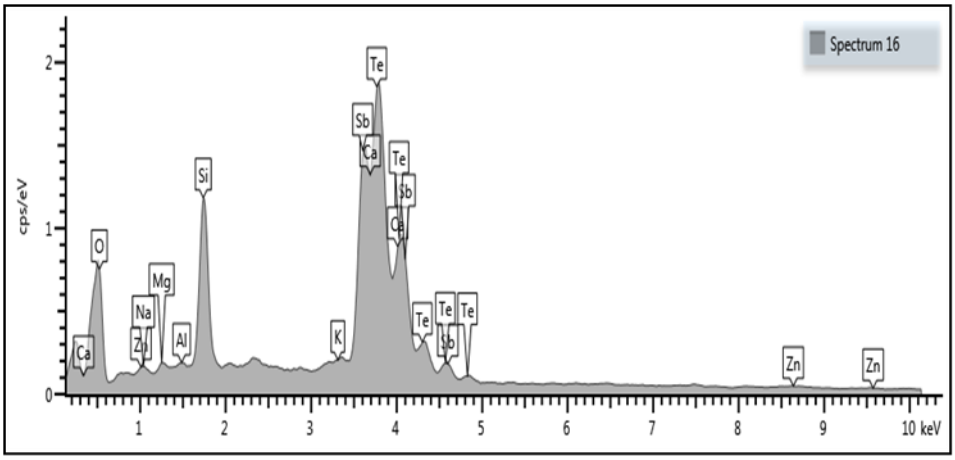

the following ratios (3%, 5%, and 7%) at a thickness of 100 nm doped with zinc prior to annealing are 2.976 nm, 1.003 nm, and 2.063 nm, respectively. This suggests that doping reduces surface roughness, which enhances the characteristics of the films' surfaces and their structural qualities [28].

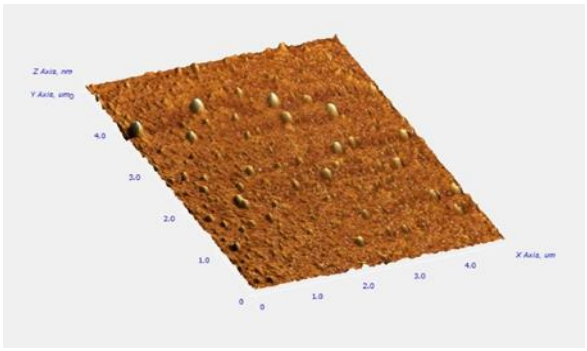

Sb_2Te_3 (100 nm) Before Annealing

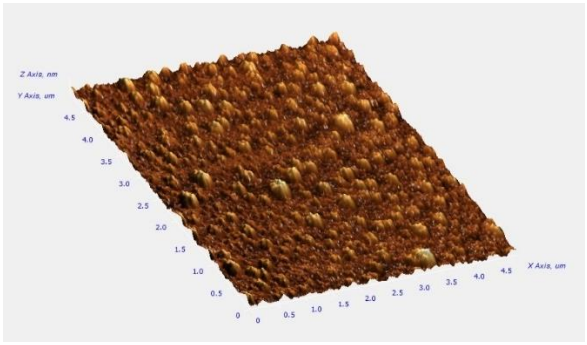

Sb_2Te_3 (200 nm) Before Annealing

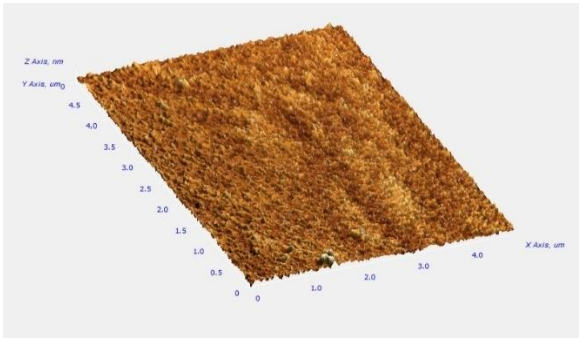

Sb_2Te_3 (300 nm) Before Annealing

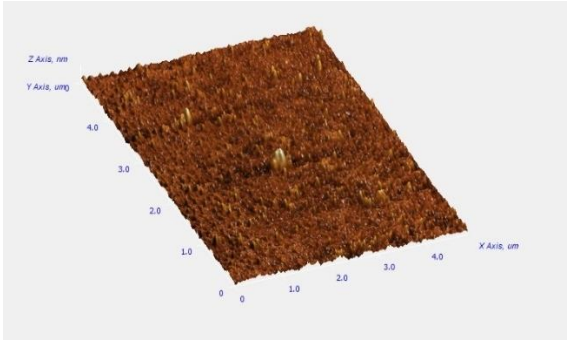

Sb_2Te_3 (100 nm) After Annealing

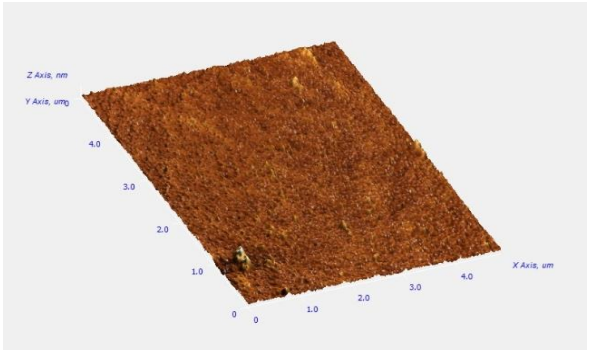

Sb_2Te_3 (200 nm) After Annealing

Figure 4. AFM images of pure Sb2Te3 films with thicknesses (100 , 200 ,300 nm) before and after annealing.

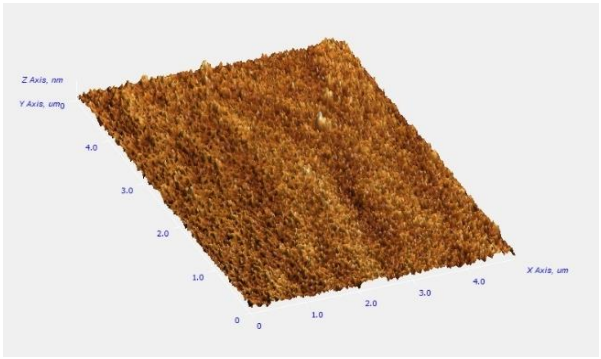

Sb_2Te_3 (300 nm) After Annealing

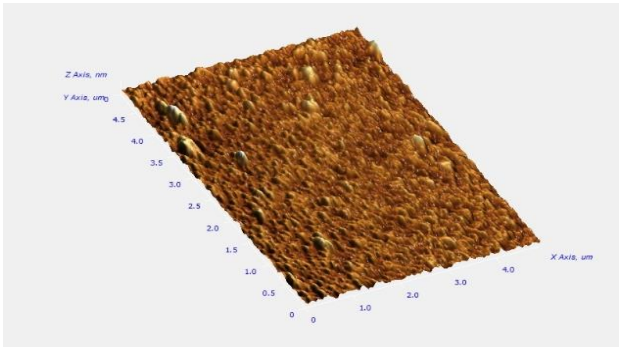

(Sb_2Te_3:3% Zn) Before Annealing

(Sb_2Te_3:5% Zn) Before Annealing

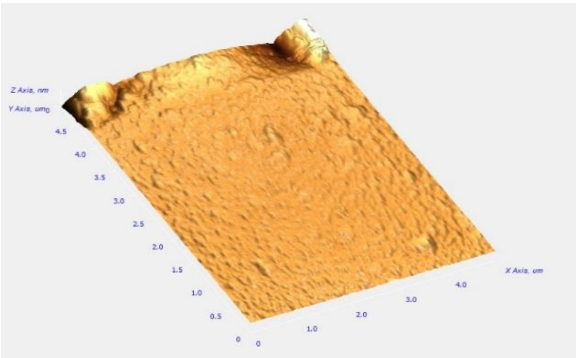

(Sb_2Te_3:7% Zn) Before Annealing

(Sb_2Te_3:3% Zn) After Annealing

(Sb_2Te_3:5% Zn) After Annealing

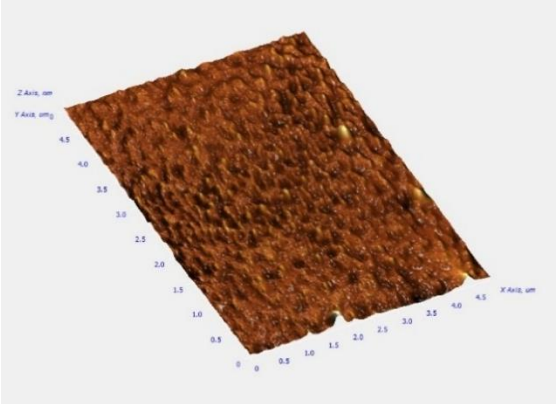

(Sb_2Te_3:7% Zn) After Annealing

Figure 5. AFM images of (Sb_2Te_3: Zn) films at concentrations of (3% ,5% ,7%) before and after annealing.

Table 3. AFM results for pure (Sb2Te3) and (Sb2Te3: Zn) films before and after annealing.

Sample	Annealing temperature	Root mean square(nm) R.M.S	Roughness average(nm) Sa
Sb_2Te_3 (100nm)	—	3.793	2.695
Sb_2Te_3 (200nm)	—	7.579	5.898
Sb_2Te_3 (300nm)	—	2.720	2.176
Sb_2Te_3 (100nm)	100 °C	2.774	2.073
Sb_2Te_3 (200nm)	100 °C	2.633	2.054
Sb_2Te_3 (300nm)	100 °C	3.089	2.464
Sb_2Te_3:3%Zn	—	3.762	2.976
Sb_2Te_3:5%Zn	—	1.275	1.003
Sb_2Te_3: 7%Zn	—	2.565	2.063
Sb_2Te_3: 3%Zn	100 °C	1.798	1.339
Sb_2Te_3: 5%Zn	100 °C	2.553	2.042
Sb_2Te_3: 7%Zn	100 °C	5.709	4.509

Optical properties

and Figure 6, shows the reflectivity before after annealing of (Sb_2Te_3) films with different thicknesses (100, 200, 300 nm), where they exhibit a decreasing reflectivity behavior with increasing wavelength within the range (200–1200 nm), followed by clear oscillations at higher wavelengths due to optical interference within the film layer. The reflectivity of the thicker films also decreases, especially at 300 nm, indicating higher absorption associated with the increased thickness of the active layer. Regarding the oscillations after 800 nm, they indicate a relative uniformity in thickness and multiple reflections between the film and the substrate, which confirms that increasing the thickness contributes to reducing reflectivity and improving absorption before annealing [29].

After annealing, the films show a general increase in reflectivity values, especially in the near-infrared region, due to improved crystallization and reduced defects and surface roughness, which decreases light scattering. The film with a thickness of 100 nm demonstrates the highest reflectivity due to lower absorption, while the thicker film (300 nm) remains less reflective due to continued higher internal absorption. In general, annealing led to a significant modification in the optical properties by improving the internal structure, which was clearly reflected in the reflectance curves [30].

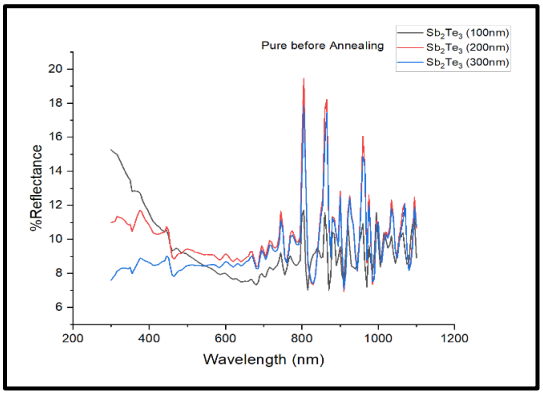

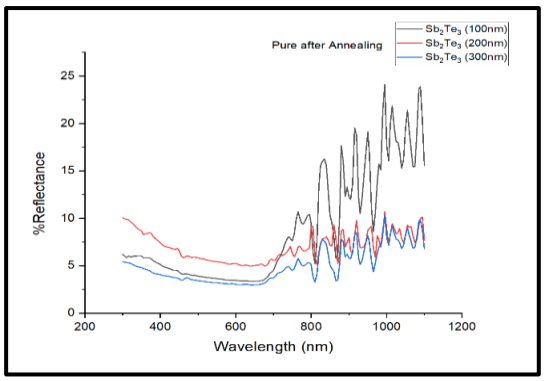

Figure 6. show optical reflectance (R%) of pure thin films Sb_2Te_3 with thicknesses (100,200 ,300 nm) before and after annealing.

Figure 7, shows the reflectance curves of (Sb_2Te_3: Zn) films doped with (3%, 5%, 7%) ratios before and after annealing. The curves show a slight decrease in reflectivity values before annealing with increasing doping levels, especially in the visible region, indicating that the addition of zinc contributed to increased optical absorption and improved the film's response to high-energy photons. The decrease of reflectivity of this product is probably caused by minor alteration of crystalline structure, by adding the components of zinc for the crystal lattice of (Sb_2Te_3), consequently the emergence of secondary energy level within the band gap with a better absorption effect [31]. After the annealing process all the curves presents a moderate increase in reflectance values as compared to pre-annealing value, especially from (800 to 1100 nm) which corresponds to an improvement in crystalline order and a reduction in surface defects after thermal treatment. Sample doped with (5%) has the highest reflectivity in most of the spectral distance, showing that this ratio is the best for finding the light absorption in our sample without losing the structural homogeneity of the film. At the higher doping concentration of (7%), the reflectivity begins to decrease again, suggesting the occurrence of crystal distortions or an increase in defects due to the higher concentration of impurities. These results indicate that annealing contributed to the activation of zinc atoms within the crystal structure and improved its stability, which in turn affected the optical properties [32].

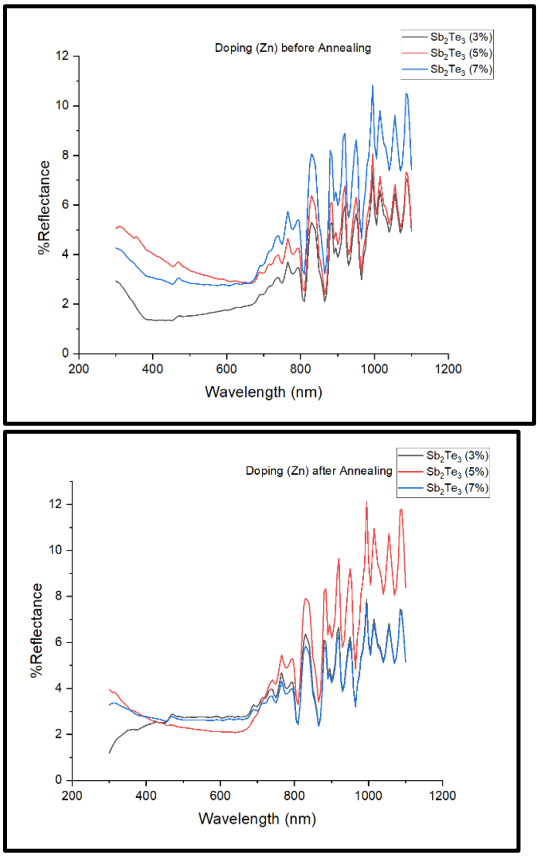

Figure 7. Optical reflectance (R%) of (Sb_2Te_3: Zn) films at concentrations of (3% ,5% ,7%) before and after annealing.

1.1 The optical bandgap (E_g)

The energy gap of pure (Sb_2Te_3) films was calculated before and after annealing based on Equation (5)[33]:

$$[F(R_\infty)hv]^2 = A(hv - E_g)^r \ldots\ldots\ldots(7)$$

As shown in Figure 8, the results showed that the energy gap values ranged between (1.6–2.1 eV) depending on the thickness and annealing

condition. It was observed from Table 4, that the energy gap slightly decreased after the annealing process for all films, and this decrease can be attributed to the improvement in the crystalline structure and the reduction in the density of defects resulting from the initial deposition. Annealing leads to the rearrangement of atoms within the crystal lattice and reduces defects and vacancies, causing a slight shift toward lower energies (Red Shift) in the absorption edge. However, after annealing, the absorption edge became clearer and most uniform, indicating a decrease in Urbach Energy resulting from electronic defects, which reflects an improvement in the optical and crystalline properties of the films. The small deviation in the energy gap is an evidence that the annealing process does not transform the chemical composition of the films in any fundamental way, but rather contributes to their structural homogeneity so that electronic transitions become more pronounced and closer to direct transitions [34]. The energy gap of (Sb_2Te_3: Zn) films at varying concentrations (3%, 5%, 7%) as prepared before annealing and after it, is shown in Figure 9. It indicates that the absorption edge prior to annealing shifts progressively towards higher energy values with a higher concentration of zinc, suggesting that the energy gap increases slightly due to the presence of zinc impurities in the crystal lattice of (Sb_2Te_3). In this respect, this phenomenon may lead to a blocking effect on the conduction levels because zinc ions are substituted with smaller radius compared to antimony or tellurium atoms, and this will cause an increase in the separation of energy levels.. The presence of zinc may also contribute to reducing the concentration of defects within the energy gap, which enhances direct electronic transition and shows a slight broadening of the optical edge [35]. And after annealing, it was observed that the absorption edge has shifted toward lower energies. This means that the energy gap has decreased slightly, and this decrease is attributed to the improvement in crystallinity and the reduction of surface defects after annealing, which reduces quantum effects and makes the structure more uniform, causing absorption to shift toward lower photonic energies [36].

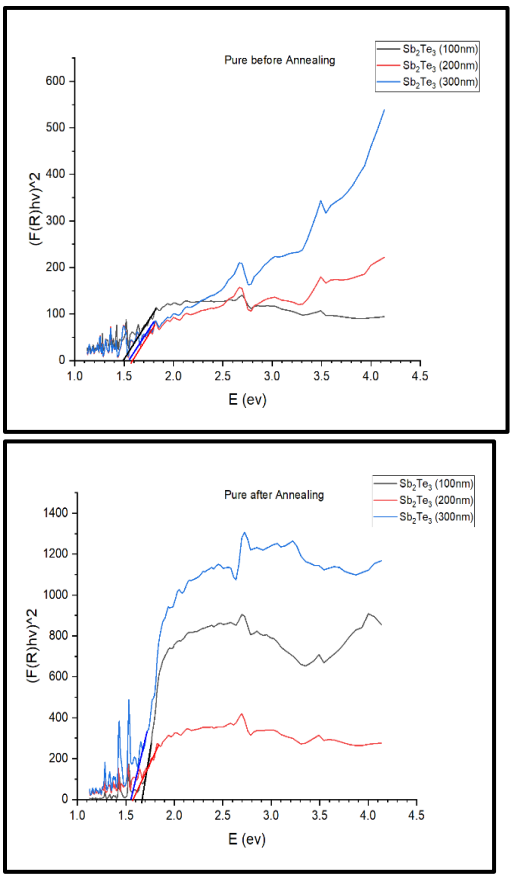

Figure 8. Energy gap of pure thin films Sb_2Te_3 with thicknesses (100,200,300 nm) before and after annealing.

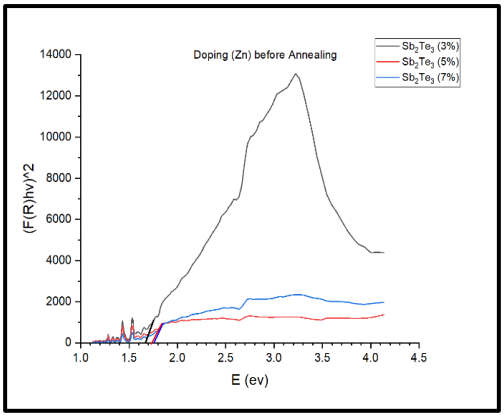

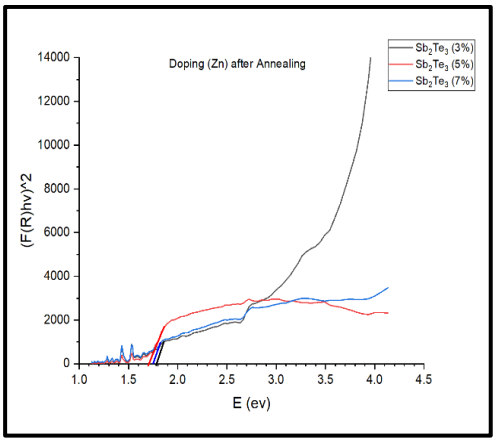

Figure 9. Energy gap of (Sb_2Te_3: Zn) films at concentrations of (3% ,5% ,7%) before and after annealing.

Table 4. Energy gap values of pure (Sb2Te3) and (Sb2Te3: Zn) films before and after annealing with different thicknesses of 100 ,200 ,300 nm.

Thickness(nm)	Annealing	Band gap (eV)	(Doping Zn)	Annealing	Band gap (eV)
Sb_2Te_3(100 nm)	---------	1.65	Sb_2Te_3: Zn 3%	----------	1.73
Sb_2Te_3(200 nm)	----------	1.70	Sb_2Te_3:Zn 5%	----------	1.80
Sb_2Te_3(300 nm)	----------	1.78	Sb_2Te_3: Zn 7%	----------	1.88
Sb_2Te_3(100 nm)	100 °C	1.68	Sb_2Te_3: Zn 3%	100 °C	1.70
Sb_2Te_3(200 nm)	100 °C	1.73	Sb_2Te_3: Zn 5%	100 °C	1.75
Sb_2Te_3(300 nm)	100 °C	1.81	Sb_2Te_3: Zn 7%	100 °C	1.82

Conclusion

Sb_2Te_3 thin films were produced with varying thicknesses and Zn doping levels (3%, 5%, 7%) using thermal evaporation technique. X-ray diffraction confirmed a hexagonal crystalline structure, indicating structural stability. Doping with zinc altered diffraction peak intensity and positions, showing zinc incorporation into the Sb_2Te_3 lattice and resulting in improved crystal quality. AFM and SEM images showed that annealing at 100 °C for one hour helped improve surface uniformity, increase grain size, and reduce roughness. Optical measurements revealed an energy band gap of 1.81 eV to 1.65 eV, typical for Sb_2Te_3,with a slight reduction in gap due to annealing, enhancing photon absorption for photovoltaic applications.

References

[1] L. I. Maissel and R. Glang, Handbook of Thin Film Technology. New York, NY, USA: McGraw-Hill, 1970.

[2] O. S. Heavens, Optical Properties of Thin Solid Films. New York, NY, USA: Dover, 1991.

[3] M. Ohring, Materials Science of Thin Films, 2nd ed. San Diego, CA, USA: Academic Press, 2002.

[4] H. Zhang, C.-X. Liu, X.-L. Qi, X. Dai, Z. Fang and S.-C. Zhang, "Topological insulators in Bi_2Se_3, Bi_2Te_3, and Sb_2Te_3: A new class of three-dimensional topological insulators," Nature Physics, vol. 5, pp. 438–442, 2009.

[5] M. Z. Hasan and C. L. Kane, "Colloquium: Topological insulators," Reviews of Modern Physics, vol. 82, no. 4, pp. 3045–3067, 2010.

[6] Y. Ando, "Topological insulator materials," Journal of Physical Society of Japan, vol. 82, no. 10, pp. 102001-1–102001-32, 2013.

[7] S. Bera, R. K. Sahu, S. K. Sinha and S. K. Tripathi, "Optical and photovoltaic properties of Sb_2Te_3 thin films," Materials Chemistry and Physics, vol. 135, no. 2-3, pp. 918–923, 2012.

[8] P. M. P. Salomé, J. P. Leitão, E. Cunha, A. F. da Cunha, P. A. Fernandes and A. F. Nogueira, "Investigation of Sb_2Te_3 thin films for solar energy conversion," Solar Energy Materials and Solar Cells, vol. 159, pp. 272–279, 2017.

[9] E. M. F. Vieira, M. A. Morales, J. A. Moreira, J. C. C. Freitas, and A. B. Bastos, "Toward enhancing the thermoelectric properties of Bi_2Te_3 and Sb_2Te_3 alloys by co-evaporation of Bi_2Te_3:Bi and Sb_2Te_3:Te," Materials, vol. 15, no. 4, 2022.

[10] R. Mendoza, J. Sastre, A. Del Oso, M. de las Á. Hernández, J. Lizardi, and G. Santana, "Pressure effects on the growth of Sb_2Te_3 thin films processed by DC and RF sputtering," IJRDO-Journal of Applied Science, vol. 5, no. 6, 2020.

[11] Jiyang Liu, Xiaolan Liu, Ke Yang, Siying He, Hongting Lu, Bing Li, Guanggen Zeng, Jingquan Zhang, Wei Li, Lili Wu, Lianghuan Feng, "Preparation and characterization of pulsed laser deposited Sb2Te3 back contact for CdTe thin film solar cell",Applied Surface Science,vol 453, pp.126-131,2018.

[12] N. H. Trung, K. Sakamoto, N. V. Toan, and T. Ono, "Synthesis and evaluation of thick films of electrochemically deposited Bi_2Te_3 and Sb_2Te_3 thermoelectric materials," Materials, vol. 10, no. 2, p. 154, 2017.

[13] B. Aboulfarah, D. Sayah, A. Mzerd, A. Giani, and A. Boyer, "MOCVD growth of Bi_2Te_3–Sb_2Te_3 layers: Effect of growth parameters on the electrical and thermoelectrical properties," Moroccan Journal of Condensed Matter, 2013.

[14] Peranio, Nicola & Winkler, Markus & Aabdin, Zainul & König, Jan & Boettner, H. & Eibl, Oliver." Room temperature MBE deposition of Bi_2Te_3 and Sb_2Te_3 thin films with low charge carrier densities". Physical Status Solidi a-Applications and Materials Science. vol 209. pp.289-293,2012.

[15] S. M. Sze, Semiconductor Devices: Physics and Technology. New York: John Wiley & Sons, 2008.

[16] M. Ohring and L. Ohring, "Mechanisms and models for thermal evaporation thin-film growth," Journal of Vacuum Science & Technology A, vol. 9, no. 2, pp. 123–130, 1991.

[17] R. F. Bunshah, Deposition Technologies for Films and Coatings. Park Ridge, NJ, USA: Noyes Publications, 1982.

[18] S. Rani, R. Sharma, and N. Goyal, "Optical and structural studies of Sb_2Te_3 thin films for thermoelectric and optoelectronic applications," Journal of Materials Science: Materials in Electronics, vol. 32, pp. 12155–12164, 2021.

[19] Park, N. W., Lee, W. Y., Hong, J. E., S.-J. Kim, and J.-S. Son, "Effect of grain size on thermal transport in post-annealed antimony telluride thin films," Nanoscale Research Letters, vol. 10, p. 20, 2015.

[20] C. B. Suryanarayana and G. Norton, "Effect of annealing on the microstructure and grain growth of thermoelectric Sb_2Te_3 thin films," Journal of Alloys and Compounds, vol. 509, no. 24, pp. 6840–6845, 2011.

[21] Z. Zhang, W. Yang, B. Wu, M. Nisar, F. Li, G.Liang, J. Luo, Y. Chen, and Z. Zheng, "A Zn-doped Sb_2Te_3 flexible thin film with decoupled Seebeck coefficient and electrical conductivity via band engineering," Chemical Science, vol. 16, pp. 3638–3645, 2025.

[22] J. Yu, W. Zhu, and H. Zhang, "Effects of Ge-doping on the structure and resistivity of Sb_2Te_3," Journal of Alloys and Compounds, vol. 253, pp. 6125-6129, 2007.

[23] Kawamura, Y., Yamashita, T., Nakanishi, Y. "Microstructural Evolution and Dislocation Behavior in Thermoelectric Sb_2Te_3 During Low-Temperature Annealing," Journal of Electronic Materials, vol. 48, pp. 5110–5118, 2019.

[24] Kumari, M., Kumar, A. "Chalcogenide-Alternating Bi_2Te_3–Sb_2Te_3 Thin Films: Structural, Microstrain and Dislocation Density Analysis," Chalcogenide Letters, vol. 19, no. 3, pp. 59–67, 2022.

[25] Rolston, N., Guicciardi, S., Kazim, S. et al. "Thickness-Dependence of Thermoelectric Properties and Maximum Output Power of Single Planar Sb_2Te_3 Films," Materials, vol. 15, no. 24, pp. 8850, 2022.

[26] M. A. Angadi, S. W. Kim, J. S. Son, and C. U. Jung, "Effect of grain size on thermal transport in post-annealed Sb_2Te_3 thin films," Journal of Applied Physics, vol. 107, no. 3, 033708, 2010.

[27] S. Li and J. Wei, "Thickness-dependent Seebeck coefficient and electrical conductivity in Sb_2Te_3 thin films," Materials Today: Proceedings, vol. 62, pp. 1156–1163, 2022.

[28] A. Shafiei, E. Marzbanrad, and S. Abedin, "Wafer-scale synthesis of topological insulator Sb_2Te_3 films," Advanced Materials Interfaces, vol. 12, no. 2, p. 2400961, 2025.

[29] J.-W. Park, S. H. Baek, T. D. Kang, H. Lee, Y.-S. Kang, J. L. F. Da Silva, and S.-H. Wei, "Optical properties of (GeTe, Sb_2Te_3) pseudobinary thin films studied with spectroscopic ellipsometry," Applied Physics Letters, vol. 93, no. 2, pp. 021914, 2008.

[30] D. Coiras, R.-N. Verrone, A. Campos, M. Cabié, L. Gallais, M. Minissale, J. Lumeau, J.-Y. Natoli, and K. Iliopoulos, "Laser annealing of Sb_2Te_3 2D layers towards nonlinear optical applications," Optics, vol. 3, no. 4, pp. 560–573, 2022.

[31] T. A. Jumah, K. M. Jalb, and H. N. Abdul-Karim, "Synthesis and Characterisation of Zinc-doped Antimony Selenide–Antimony Thin Films," Iraqi Journal of Science, vol. 62, no. 10, pp. 3552–3559, 2021.

[32] N. Q. Adanan, S. Wredh, Md. A. Rahman, J. K. W. Yang, and R. E. Simpson, "Continuously tunable optical states of highly textured Sb_2Te_3," Optical Materials Express, vol. 15, no. 9, pp. 2289–2298, 2025.

[33] J. Tauc, R. Grigorovici and A. Vancu, "Optical properties and electronic structure of amorphous germanium," Physica Status Solidi, vol. 15, no. 2, pp. 627–637, 1966.

[34] K. U. Rehman, M. F. Khan, A. Mahmood, F. Ahmad, M. Y. Nadeem and S. Arshad, "Effect of annealing on the structural and optical properties of Sb_2Te_3 thin films," Chalcogenide Letters, vol. 8, no. 7, pp. 401–407, 2011.

[35] A. B. Dinkar, S. D. Delekar, V. S. Sangawar and C. A. Pawar, "Optical, structural and electrical properties of annealed Sb_2Te_3 films," Journal of Alloys and Compounds, vol. 509, pp. 5783–5788, 2011.

[36] S. S. Shinde, P. S. Shinde, S. R. Nalage, K. Y. Rajpure and C. H. Bhosale, "Optical and structural properties of Zn-doped Sb_2Te_3 thin films," Journal of Materials Science: Materials in Electronics, vol. 24, no. 2, pp. 654–660, 2013.